Rayleigh and mie scattering

Lockwood, David J.

Publisher's version / Version de l'éditeur:
https://doi.org/10.1007/978-3-642-27851-8_218-2
Encyclopedia of Color Science and Technology, 2016-04-06

Rayleigh and Mie Scattering[1]

David J. Lockwood, National Research Council Canada
Ottawa, ON, Canada
david.lockwood@nrc-cnrc.gc.ca

Synonyms

Rayleigh scattering – elastic scattering, elastic light scattering
Mie scattering – Mie theory, Mie solution, Lorenz-Mie theory, Lorenz-Mie-Debye theory

Definitions

Rayleigh scattering refers primarily to the elastic scattering of light from atomic and molecular particles whose diameter is less than about one-tenth the wavelength of the incident light. Rayleigh line refers to the unshifted central peak observed in the spectroscopic analysis of scattered light. Mie scattering refers primarily to the elastic scattering of light from atomic and molecular particles whose diameter is larger than about the wavelength of the incident light. Thomson scattering is elastic scattering of light from free electrons. Raman scattering is inelastic scattering of light from objects whereby the scattered photon has a lower (Raman Stokes scattering) or higher (Raman anti-Stokes scattering) energy than the incident photon.

Introduction

From ancient times, people have gazed up at the sky in daylight and asked the perennial question "Why is the sky blue?" [1]. Other similar and related questions are "Why is the night sky black?", "Why are sunrises and sunsets red?", and "Why are the clouds white?". Rayleigh [2-5] and Mie scattering [6] lie behind the long sought answers to all such questions about the colors seen in the sky.

The phenomenon called Rayleigh scattering is named after its discoverer, John William Strutt, 3rd Baron Rayleigh (Fig. 1), a physicist who is known for a number of significant scientific discoveries that he made towards the end of the 19th Century including the discovery of argon, an achievement for which he earned the Nobel Prize for Physics in 1904. However, the use of the term "Rayleigh scattering", in general, and also "Rayleigh line", in specific use in light scattering spectroscopy, has been controversial in the past and has led to some confusion [7]. These nomenclature issues will be clarified in the following discussion. It is also noteworthy that Rayleigh contributed widely to scattering theory in eight different categories; for an overview of these different contributions, see Reference [8]. However, this article is limited to a description of classical Rayleigh scattering of light from single small objects such as molecules and atoms. Thus, it is ignoring coherence effects that arise in solids, liquids, and gases at atmospheric pressure or even in free electrons where it is known as Thomson scattering.

The scientific history behind the development of the term "Mie scattering" or "Mie theory" is convoluted [9]. Mie theory solves one of the most important problems in optics; the absorption and scattering of light by a small sphere of arbitrary size and refractive index. In 1908, Gustav Mie (Fig. 2) published his now famous paper on the simulation of the color effects connected with colloidal Gold

[1] In celebration of the United Nations International Year of Light 2015.

particles [6] wherein he applied Maxwell's electromagnetic theory to calculate light scattering from small spherical particles. He was not the first to perform this calculation, as similar investigations were also carried out and published earlier in 1863 by Alfred Clebsch and in 1890 by Ludvig Lorenz, and soon afterwards in 1909 by Peter Debye [9]. However, Mie was the first to apply Maxwell's equations to finding a solution and his name is now firmly attached to the theory, which is sometimes also called Lorenz-Mie theory and Lorenz-Mie-Debye theory.

Classical Description

Rayleigh treated the scattering of light by a spherical particle, whose diameter is much smaller than that of the wavelength of light. It is generally accepted that this size regime applies for particles (or molecules) of size less than $1/10^{th}$ the vacuum wavelength, λ, of the incident light. Rayleigh considered a plane wave incident on a dielectric sphere of radius r and of relative permittivity (dielectric constant) ε, as illustrated in Fig. 2 [10]. The probability that the sphere scatters light at angle ϑ is proportional to the differential scattering cross section, $d\sigma(\theta)/d\Omega$, which is defined as the ratio of the power scattered into the solid angle $d\Omega$ between ϑ and $d\vartheta$ (see Fig. 3) to the incident power per unit area. For unpolarized incident light, the differential cross section becomes [10]

$$d\sigma(\theta)/d\Omega = (1/2)\,(2\pi n_0/\lambda)^4\, r^6\, [(\varepsilon-\varepsilon_0)/(\varepsilon+2\varepsilon_0)]^2\,(1+\cos^2\theta), \qquad (1)$$

where ε_0 is the relative permittivity and n_0 the refractive index of the medium surrounding the sphere of refractive index n. Integrating this equation over the entire solid angle yields the total cross section:

$$\sigma_R = (8\pi/3)\,(2\pi n_0/\lambda)^4\, r^6\, [(\varepsilon-\varepsilon_0)/(\varepsilon+2\varepsilon_0)]^2. \qquad (2)$$

The intensity I_R of the Rayleigh scattered light is given by [11]

$$I_R = I\,(2\pi n_0/\lambda)^4\,(r^6/2D^2)\,[(\varepsilon-\varepsilon_0)/(\varepsilon+2\varepsilon_0)]^2\,(1+\cos^2\theta), \qquad (3)$$

where I is the intensity of the unpolarized incident light and D is the distance between the particle and the observer.

It is now possible to explain why the sky overhead looks bright blue to an observer such as Dante Alighieri's effigy in Florence, Italy, as illustrated perfectly in Fig. 4. Equation (4) indicates that the Rayleigh scattering intensity varies as the fourth power of the inverse wavelength of the incident light. This is known as Rayleigh's law. For example, the intensity of Rayleigh scattering at 400 nm in the blue part of the visible spectrum is higher by a factor of 9.38 compared with that at 700 nm in the red portion of the spectrum. So, when considering Rayleigh scattering of visible sunlight from molecules in the air, it is clear that blue light will be brighter than red light. Conversely, at sunset, when the sunlight travels further though the earth's atmosphere, more blue light is scattered out of the beam path than red light, so the sunset glows red (Fig. 5). The $(1+\cos^2\theta)$ term in Equation (3) contains the angular dependence of the scattering, and indicates that Rayleigh scattering intensity at 90° is one-half that in the forward or backward directions.

For particle sizes larger than λ, Mie scattering predominates [6, 12] and for particles that are much larger than λ a third type of atmospheric scattering, known as non-selective scattering, occurs [13]. A description of this last type of scattering, which can be considered as comprising a combination of Mie scattering, absorption, and multiple scattering, is outside the scope of this article. Non-selective scattering is not wavelength dependent and is the primary cause of haze in the lower atmosphere. Water droplets and large dust particles can cause this type of scattering.

A mathematical description of the physics of Mie scattering is the result of a considerably more complicated calculation than that needed for Rayleigh scattering [12]. The calculation involves considering a plane wave incident on the sphere and a spherical scattered wave. The total scattering cross section, σ_M, can be expressed in the form of an infinite series as [10]

$$\sigma_M = (\lambda^2/2\pi n_0^2) \sum (2m + 1)(|a_i|^2 + |b_i|^2), \quad (4)$$

where the summation is from $i = 1$ to infinity, and the coefficients a_i and b_i are expressed in terms of spherical Hankel functions and spherical Bessel functions of the first kind; these functions are dependent on the magnetic permeabilities of the sphere and surrounding medium and the values of parameters $m = n/n_0$ and $x = 2\pi n_0 r/\lambda$, which is termed the size parameter. Representative results from calculations of the Rayleigh and Mie scattering cross sections using Equations (2) and (4), respectively, are shown in Fig. 6 in terms of the scattering efficiency $Q = \sigma/\pi r^2$. This figure demonstrates that for small spheres with $mx << 1$, ($x = 2\pi n_0 r/\lambda$ and $m = n/n_0 = 1.59/1.33$), the scattering efficiencies of Rayleigh and Mie scattering are very nearly the same, whereas for larger spheres with high mx values the behavior is completely different. The Mie scattering efficiency departs from the Rayleigh λ^{-4} behavior and approaches a limiting value of $Q = 2$, as a consequence of the "extinction paradox" related to equal geometrical and diffraction contributions to the cross section [10]. The diffraction contribution is most readily discerned at a distance from the sphere and is strongly peaked in the forward direction. Thus Mie scattering produces a scattering pattern like an antenna lobe with a forward lobe that becomes more intense and sharper with increasing particle size. For larger particle sizes, as Fig. 6 shows, Mie scattering is not strongly wavelength dependent. This is the reason that such scattering from water droplets in clouds, mist, or fog, produces white light, as can be seen in Fig. 4 in the lower part of the sky behind the lion. Likewise, due to its larger forward lobe, Mie scattering produces the whitish glare that is seen surrounding the sun when large particulate matter is present in the air.

Quantum Description

In describing Rayleigh scattering, only the classical interaction of light with small particles has been considered so far. However, for very small particles, a proper account of Rayleigh scattering requires a quantum mechanical description. This is given, for example, by Placzek [14] in the early days of quantum theory and, in a more modern setting, by Loudon [15], which is followed here. Scattering of light by an atom or molecule is a second-order radiative process: a quantum (or photon) of energy $\hbar\omega$ (ω is the angular frequency and $\hbar = h/2\pi$, where h is Planck's constant) of the incident light beam is destroyed and a quantum of scattered light of energy $\hbar\omega_s$ is created. When $\omega_s = \omega$, the process is called elastic scattering or Rayleigh scattering in the nomenclature of this field of research, which is where the

use of terminology leads to naming confusions for different scattering processes [7]. When $\omega_s \neq \omega$, the process is called inelastic scattering or Raman scattering; the energy difference thus created is accommodated by the atom or molecule that is involved in the scattering process. Energy may be transferred to, or taken from, the atom or molecule via an electronic transition, in which case it is call Raman Stokes, or Raman anti-Stokes, scattering. These three different electronic energy transition processes are illustrated in Fig. 7. Electronic transitions can occur between any states, but usually arise from or terminate at the ground state or thermally populated higher states and the excited states are usually virtual states; that is, they are not stationary states of the system. However, if the energy of the incident or scattered light is close to or at a stationary energy state, electronic resonant scattering occurs.

After a full quantum-mechanical derivation, the differential cross section of the elastic scattering of light by an atom, $d\sigma/d\Omega$, can be written as [15]

$$d\sigma/d\Omega = (e^4\omega^4/16\pi^2\varepsilon_0{}^2\hbar^2c^4)\ |\sum\{[\varepsilon_s.D_{1i}\varepsilon.D_{i1}/(\omega_i - \omega)] + [\varepsilon.D_{1i}\varepsilon_s.D_{i1}/(\omega_i + \omega)]\}|^2, \quad (5)$$

for the case of the atom returning to its ground state $i = 1$ at the conclusion of the scattering event. The summation index i includes all the eigenstates of the atomic Hamiltonian. Note that the cross section varies as the fourth power of the frequency of the incident light, as in the classical result. This equation is a simplified form of the general Kramers-Heisenberg formula for the differential cross section that also covers inelastic (Raman) scattering [15] and forms the basis for quantum-mechanical scattering theory. In Equation 5, the summation is carried out over all stationary states i; c is the velocity of light, e the electron charge, $\boldsymbol{\varepsilon}$ and $\boldsymbol{\varepsilon}_s$ are the unit polarization vectors for the incident and scattered light, and D is the sum of the electron coordinates and is proportional to the atomic-dipole moment. Evaluating the matrix elements that determine D is not trivial and has only been performed for simple systems such as atomic hydrogen [16].

Equation 5 may be simplified under two limiting conditions. The first is where ω is much larger than an atomic excitation frequency ω_i, but much less than $mc^2/\hbar$ where m is the electron mass. In this high frequency limit (corresponding to Thomson scattering) the cross section reduces simply to [15]

$$d\sigma/d\Omega = Z^2r_e{}^2(\varepsilon.\varepsilon_s)^2 \qquad (\text{for } \omega >> \omega_i) \quad (6)$$

where Z is the number of electrons in the atom and $r_e = e^2/4\pi\varepsilon_0mc^2$ is the classical electron radius. Interestingly, this result from quantum theory for the elastic scattering cross section in the high frequency limit is identical to that obtained from classical theory for Thomson scattering [15].

The second limiting case is where ω is much smaller than all atomic excitation frequencies ω_i, in which case Equation 5 becomes [15]

$$d\sigma/d\Omega = (e^4\omega^4/16\pi^2\varepsilon_0{}^2\hbar^2c^4)\ |\sum(\varepsilon_s.D_{1i}\varepsilon.D_{i1} + \varepsilon.D_{1i}\varepsilon_s.D_{i1})/\omega_i|^2. \quad (7)$$

This expression for the cross section in the low frequency limit can readily be evaluated for atomic hydrogen, yielding [15, 16]

$$d\sigma/d\Omega = (81r_e^2/64)(\omega/\omega_R)^4(\varepsilon.\varepsilon_s)^2 \qquad (\text{for } \omega << \omega_i), \tag{8}$$

where $\hbar\omega_R = me^4/32\pi^2\varepsilon_0^2\hbar^2$ is the ground state binding energy of hydrogen.

The full expression given in Equation 5, for the elastic scattering cross section has been determined for hydrogen by Gavrila [16]. His tables of results for the magnitude of the scattering matrix element as a function of the frequency of the incident light have been graphically depicted by Loudon [15] and some results are illustrated in Fig. 8. For this case, the differential cross section can be written as [15]

$$d\sigma/d\Omega = r_e^2 |M_1|^2 (\varepsilon.\varepsilon_s)^2, \tag{9}$$

where

$$M_1 = (m\omega^2/\hbar) \sum(2\omega_i |X_{1i}|^2)/(\omega_i^2 - \omega^2) \tag{10}$$

and X_{1i} are the appropriate electric-dipole matrix elements. Note that in the frequency region below ω_R there are several strong electronic transition resonances evident (only those up to the fifth excited state were calculated by Gavrila) separated by zeros in the differential cross section. Such resonances could not be predicted from the classical model used by Rayleigh. The inclusion of radiative damping in the theory removes the infinite values from the cross section and the accompanying zeroes evident in Fig. 8. Note also that at high frequencies the cross section value approaches that of Thomson scattering, as given by Equation (6) with Z = 1, and eventually reaches it when $\omega >> \omega_i$.

Representative Scattering Media

Here we review Rayleigh and Mie scattering processes at work in different media of interest, including solids, liquids, and gases, and provide some examples of their practical applications.

In fluids, conventional Rayleigh scattering is most commonly observed. Although proof of Rayleigh's law in gases was obtained quite early on [2, 17], at just a few isolated wavelengths, it was not until later that detailed information was obtained over a wide wavelength range. In 1973, Stone [18] reported on measurements of the Rayleigh scattering from CCl_4 and C_2Cl_4 as a function of wavelength between 600 nm and 1060 nm by placing the liquid sample in a hollow fused-quartz fiber and measuring the light scattered by the liquid through the fiber wall. Stone determined that the scattering loss rate was 25 dB/km for CCl_4 and 68 dB/km for C_2Cl_4 at 632.8 nm and that the scattering loss rate followed a λ^{-4} dependence over the entire spectral range.

As mentioned in the Introduction, Rayleigh scattering is most commonly encountered in nature with the spectacular variations in color of the sky during the day and at sunset. In the absence of these scattering effects from atmospheric gases, the sky would be black, just like in outer space (Fig. 9). In practical applications, Rayleigh scattering from gaseous molecules is becoming an increasingly useful tool for diagnostic purposes. The use of Rayleigh imaging is particularly advantageous for visualizing the complex flow fields in fluid dynamics and combustion phenomena associated with shock waves and boundary layer structures having large density fluctuations [19]. In these measurements, quantitative

information on these complex flow structures is generated by using high-power short-pulse lasers that freeze the density field in time.

In solids, there are many examples of Rayleigh scattering at work. For example, Rayleigh scattering is mainly responsible for the blue appearance of opalescent materials when viewed under white light, although photonic band gap effects related to their microscopic structure frequently introduce striking color variations in their appearance, as can be seen in Fig. 10. The transmission of optical signals in optical fibers [20] and within microspheres or microdisks [21] is strongly affected by optical scattering processes including significant Rayleigh scattering. Glass fibers are disordered materials that exhibit microscopic variations in their density and refractive index. Rayleigh scattering from these fluctuations results in unwanted energy losses in optical transmission through the fiber with an attenuation coefficient, α_R given by [20, 21]

$$\alpha_R = (8\pi^3/3\lambda^4)n^8p^2kT\beta_T \qquad (11)$$

where n is the fiber refractive index, p the photoelastic coefficient of the glass, k the Boltzmann constant, and β_T the isothermal compressibility, and T is a fictitious temperature at which the density fluctuations are "frozen" into the glass (~1500 K for fused silica). Note that as the contribution of Rayleigh scattering to the attenuation coefficient scales with the inverse fourth power of the wavelength, the Rayleigh scattering losses predominate at shorter wavelengths. A more unusual example is the observation of recoilless Rayleigh scattering by atoms in solids. This has been observed, for example, by employing equipment designed for Mossbauer effect studies (i.e., photon sources and analyzers with extreme selectivity in energy) to observe Rayleigh scattering in Pt, Al, graphite, and paraffin using an incident light energy of 23.8 keV [22].

Unusual Rayleigh scattering effects can also be seen in solids. For example, optical studies of gases contained in nanoporous materials produced in a sample with 70 nm diameter pores shows a λ^{-4} Rayleigh-type decay of the scattering coefficient with increasing wavelength [23]. Measurements of light-scattering spectra from rutile structure fluorides using circularly polarized incident light, have revealed Rayleigh optical activity. This occurs when the incident light is tilted away from the crystal c-axis direction of the tetragonal crystal structure [24]. Rayleigh optical activity is observed experimentally through a difference in the intensity of the Rayleigh scattering when excited with right and left circularly polarized incident light. The Rayleigh circular intensity differential (CID), Δ_α, is defined by

$$\Delta_\alpha = (I_\alpha^R - I_\alpha^L)/(I_\alpha^R + I_\alpha^L) \qquad (12)$$

where I_α^R and I_α^L are the scattered light intensities with α polarization due to right and left circularly polarized incident light, respectively. The dependence of the CID spectrum on small rotations of the crystal about the laboratory y axis was measured in optically transparent MgF_2 and also in crown glass for reference purposes. For the case of the crystal $c(a)$ axis nearly aligned along the direction of the incident(scattered) monochromatic laser light, the strong dependence of the Rayleigh CID spectrum on the crystal angle is shown in Fig. 11. Most importantly for assignment purposes, the CID changes sign as the crystal is rotated through the true c-axis alignment at $\theta_e = -0.7°$. Notably, no CID is observed for small rotations of the crystal about the orientation where the incident light and scattered light

propagate perpendicular to the optic (c) axis; nor is any CID observed from the crown glass. These results indicate that the Rayleigh scattering CID observed in the MgF_2 crystal is due to depolarization effects associated with its birefringence and not polarization-dependent scattering cross sections, as confirmed theoretically [24].

Mie scattering is also found everywhere in nature: in the lower atmosphere, as noted above, in fluids like milk and latex paint, and even in biological tissue. In the latter case, Mie theory has been applied to determine if scattered light from appropriately treated tissue can be used to diagnose cancerous from healthy cells [25, 26]. Mie scattering is used in particle size determination for particles in non-absorbing media [27], in the determination of the oil concentration in polluted water [28], in parasitology [9], and in the design of metamaterials [30].

In summary, it is evident that Rayleigh and Mie scattering are ubiquitous, being found in the everyday and colorful optical wonders that surround us.

References

1. P. Lilienfeld, "A blue sky history", Optics Photonics News, 15(6), 32-39 (2004). http://dx.doi.org/10.1364/OPN.15.6.000032
2. J.W. Strutt (1871) "On the light from the sky, its polarization and colour," Philosophical Magazine, series 4, vol.41, pages 107-120.
3. J.W. Strutt (1871) "On the light from the sky, its polarization and colour," Philosophical Magazine, series 4, vol.41, pages 274-279.
4. J.W. Strutt (1871) "On the scattering of light by small particles," Philosophical Magazine, series 4, vol. 41, pages 447-454.
5. J.W. Strutt (1899) "On the transmission of light through an atmosphere containing small particles in suspension, and on the origin of the blue of the sky," Philosophical Magazine, series 5, vol. 47, pages 375-384.
6. G. Mie, (1908). "Beiträge zur Optik trüber Medien, speziell kolloidaler Metallösungen". Annalen der Physik 330 (3): 377–445.
7. A. T. Young, "Rayleigh scattering," Phys. Today 35(1), 42–48, 1982.
8. V. Twersky, "Rayleigh Scattering", Applied Optics 3, 1150-1162, 1964.
9. W. Hergert and T. Wriedt, The Mie Theory, Springer-Verlag, Berlin (2012). DOI: 10.1007/978-3-642-28738-1_2
10. A. J. Cox. A. J. DeWeerd, and J. Linden, "An experiment to measure Mie and Rayleigh total scattering cross sections", Am. J. Phys. 70, 620-625 (2002).
11. W. Hayes and R. Loudon, Scattering of Light by Crystals, Wiley-Interscience, New York (1978), p. 2.
12. C. F. Bohren and D. R. Huffman, (1983). Absorption and scattering of light by small particles. New York: Wiley-Interscience.
13. J. M. Wallace and P. V. Hobbs, Atmospheric Science: An Introductory Survey, Academic Press, Orlando, 1977.

14. G. Placzek, "The Rayleigh and Raman Scattering", in E. Marx, Ed., Handbuch der Radiologie, Vol. 6, Part 2, Akademische Verlagsgesellschaft, Leipzig (1934), pp. 209-374.
15. R. Loudon, The Quantum Theory of Light, Oxford University Press, London, (1973), Chapt. 11.
16. M. Gavrila, "Elastic scattering of photons by a hydrogen atom", Phys. Rev. 163, 147-155 (1967).
17. J. Cabannes, "Sur la diffusion de la lumière par l'air", C. R. Acad. Sci. 160, 62-63 (1915).
18. J. Stone, "Measurement of Rayleigh scattering in liquids using optical fibers", Applied Optics 12, 1824-1827 (1973). dx.doi.org/10.1364/AO.12.001824
19. R. B. Miles, W. R. Lempert, and J. N. Forkey, "Laser Rayleigh scattering", Meas. Sci. Technol. 12, R33–R51 (2001).
20. M. E. Lines, "Scattering losses in optic fiber materials. I. A new parametrization", J. Appl. Phys. 55, 4052-4057 (1984); doi: 10.1063/1.332994
21. M. L. Gorodetsky, A. D. Pryamikov, and V .S. Ilchenko, "Rayleigh scattering in high-Q microspheres", J. Opt. Soc. B 17, 1051-1057 (2000).
22. C. Tzara and R. Barloutaud, "Recoilless Rayleigh scattering in solids", Phys. Rev. Lett. 4, 405-406 and "Erratum" 539 (1960).
23. T. Svensson and Z. Shen, "Laser spectroscopy of gas confined in nanoporous materials", Appl. Phys. Lett. 96, 021107 (2010).
24. K. R. Hoffman, W .M. Yen, D. J. Lockwood and P. E. Sulewski, "Birefringence-Induced Vibrational Raman and Rayleigh Optical Activity in Uniaxial Crystals," Phys. Rev. B 49, 182 (1994).
25. M. C. Tsai, T. L. Tsai, D. B. Shieh, H. T. Chiu, and C. Y. Lee, "Detecting HER2 on cancer cells by TiO2 spheres Mie scattering", Anal Chem. 2009 Sep 15;81(18):7590-6. doi: 10.1021/ac900916s.
26. Meng Wang, Min Cao, ZhiRui Guo, and Ning Gu, "Generalized multiparticle Mie modeling of light scattering by cells", Chinese Science Bulletin July 2013, Volume 58, Issue 21, pp 2663-2666.
27. B. Gompf and R. Pecha, (May 2000). "Mie scattering from a sonoluminescing bubble with high spatial and temporal resolution". Physical Review E 61 (5): 5253–5256.
28. H. Lindner, G. Fritz, and O. Glatter (2001). "Measurements on Concentrated Oil in Water Emulsions Using Static Light Scattering". Journal of Colloid and Interface Science 242: 239.
29. Y. M. Serebrennikova, J. Patel, and L. H. Garcia-Rubio, (2010). "Interpretation of the ultraviolet-visible spectra of malaria parasite Plasmodium falciparum". Applied Optics 49 (2): 180–8.
30. Q. Zhao, J. Zhou, F. L. Zhang, and D. Lippens, (2009). "Mie resonance-based dielectric metamaterials". Materials Today 12 (12): 60–69. doi:10.1016/S1369-7021(09)70318-9.

Figures

Figure 1. Lord Rayleigh (1842-1919); ca. 1870.

Figure 2. Gustav Mie (1868-1957).

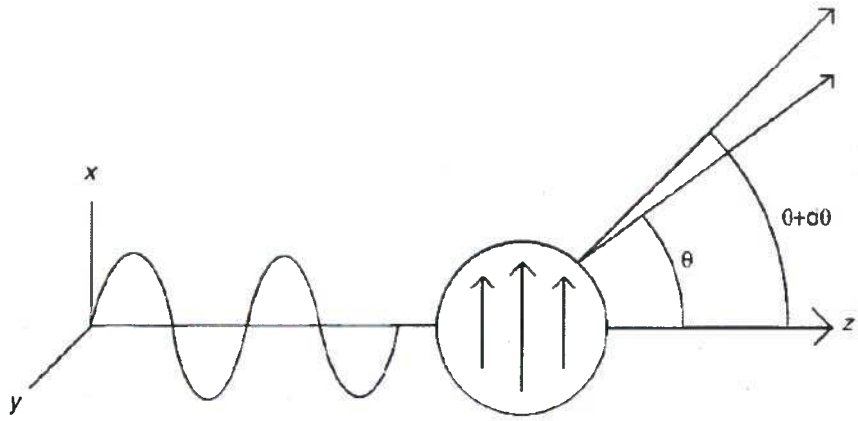

Figure 3. A plane wave polarized in the x-z plane is incident on the dielectric sphere from the left along the z direction. The arrows on the sphere denote the polarization of the dielectric material. Part of the scattered wave is shown scattered between angle θ and θ+dθ. After Ref. [10].

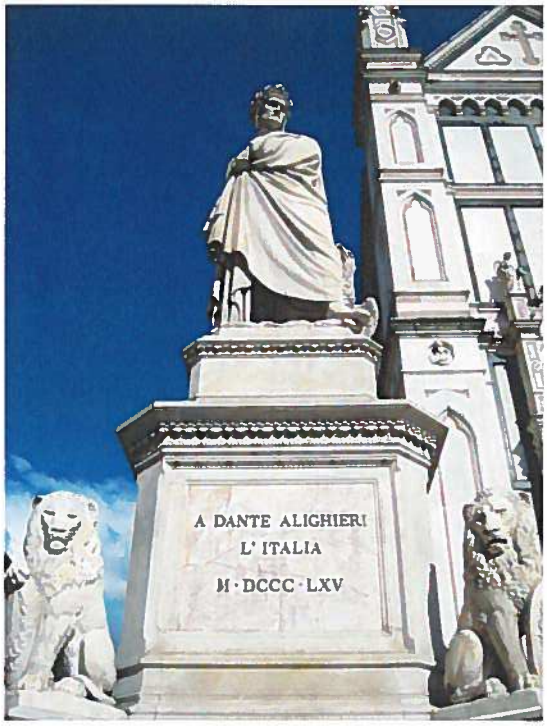

Figure 4. Dark blue skies overhead in Florence, Italy: Statue of Dante in the Piazza di Santa Croce in Florence (Enrico Pazzi, 1865). Copyright Lilia R. Lockwood.

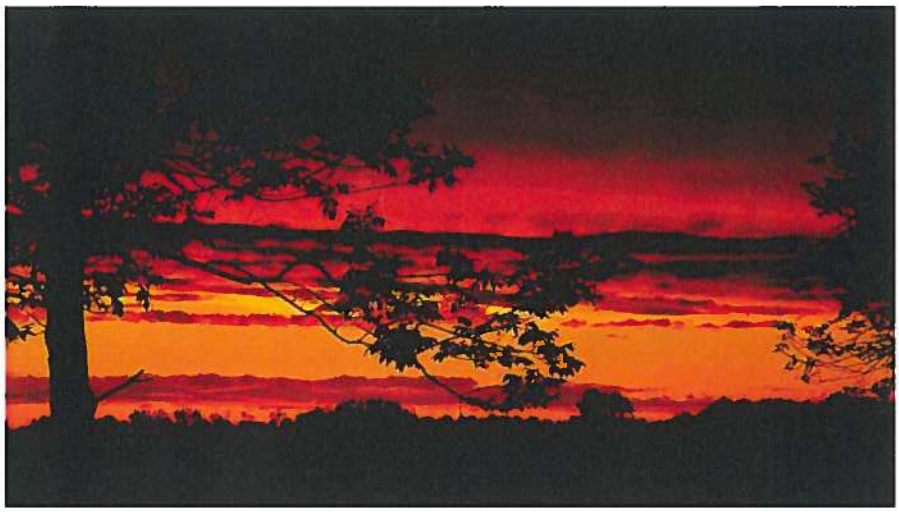

Figure 5. This photograph of the sunset seen through clouds illustrates both Rayleigh and Mie scattering. Copyright Terry Cyr.

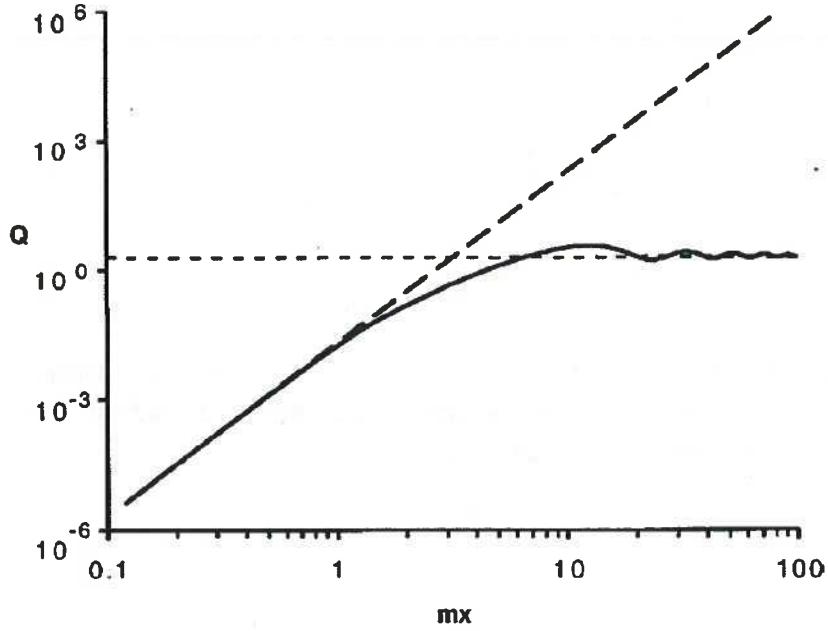

Figure 6. Scattering efficiency $Q = \sigma/\pi r^2$ versus mx ($x = 2\pi n_0 r/\lambda$ and $m = n/n_0 = 1.59/1.33$) for Rayleigh (dashed curve) and Mie (solid curve) scattering. The dotted line indicates the limiting value of $Q = 2$. After Ref. [10].

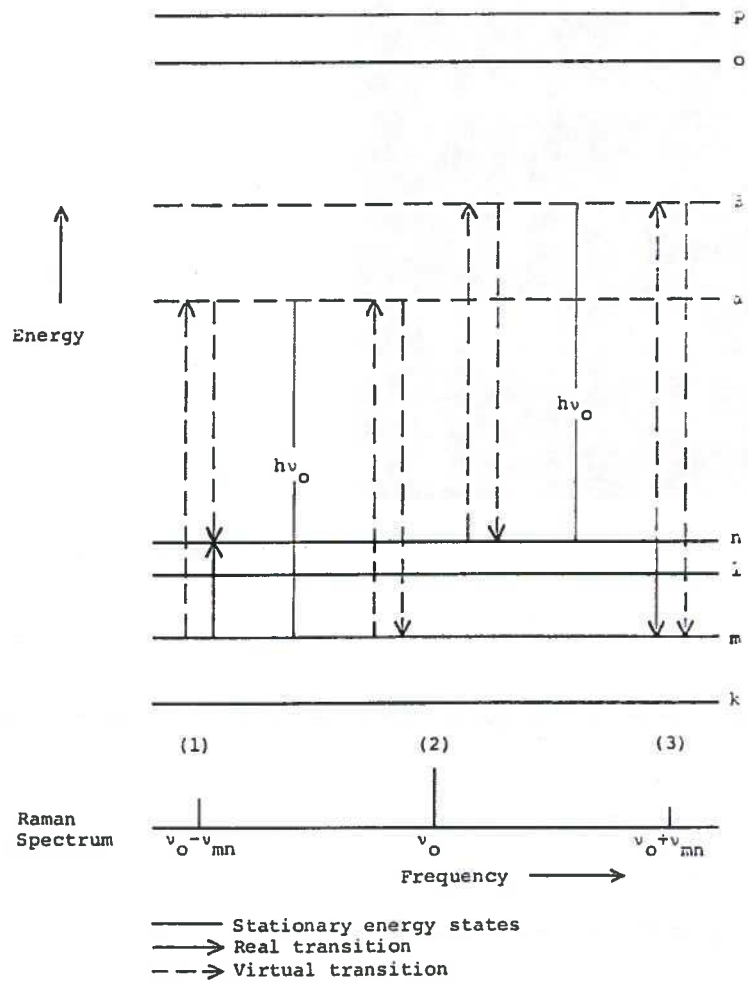

Figure 7. Quantum energy level transition representation of (1) Raman Stokes scattering, (2) Rayleigh scattering, and (3) Raman anti-Stokes scattering. The corresponding peaks created in the light scattering spectrum are shown below the three sets of different virtual transitions.

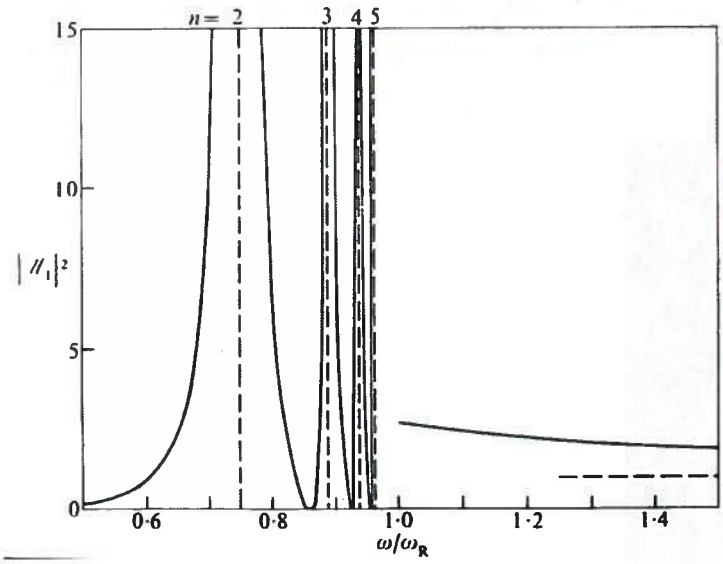

Figure 8. Frequency dependence of the elastic scattering matrix element $|M_1|^2$ for a hydrogen atom. The vertical dashed lines show the positions of resonances with the n = 2, 3, 4, and 5 electronic excited states. The horizontal dashed line shows the limiting value of $|M_1|^2$ for $\omega >> \omega_R$ in the Thomson scattering region. From Ref. [15] after the work of M. Gravila [16].

Figure 9. A composite photograph of the Earth viewed from space showing white light scattering from water droplets in clouds and the surrounding blackness of space. Copyright NASA Goddard Space Flight Center.

Figure 10. Rayleigh scattering of white incident light results in the blueish-tinged hazy appearance of the Australian opal. Copyright David J. Lockwood.

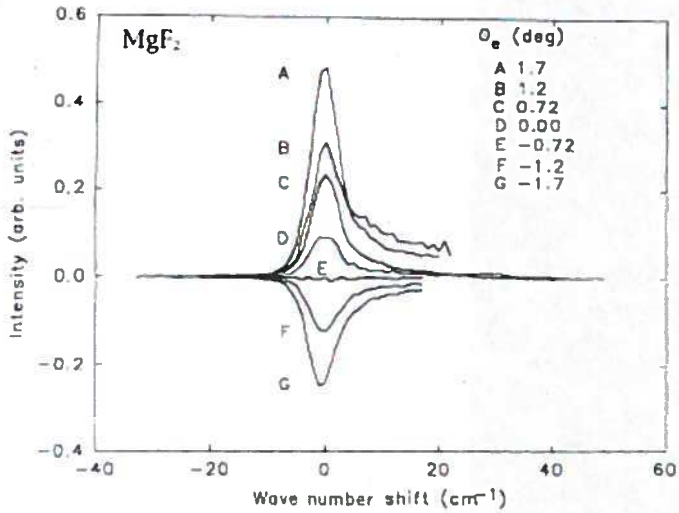

Figure 11. CID spectrum of the Rayleigh scattering in MgF_2 with the crystal rotated by angle θ_e around the laboratory *y* (crystal *a*) axis. The crystal *c* axis is in near alignment with the laboratory *z* axis. After Ref. [24].